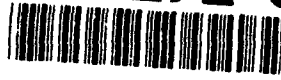


**AD-A272 386**



12

OFFICE OF NAVAL RESEARCH

Contract N00014-82-0280

Task No. NR413E001

TECHNICAL REPORT NO. 59

Direct Images of Thermal Disorder in the Cl-Si and H-O-Si Chemisorption Bond on  
Si(100)

by

Q. Gao, Z. Dohnalek, C.C. Cheng, W.J. Choyke and J.T. Yates, Jr.

Submitted To

Surface Science

Surface Science Center  
Department of Chemistry  
University of Pittsburgh  
Pittsburgh, PA 15260

October 27, 1993

Reproduction in whole or in part is permitted for any  
purpose of the United States Government

This document had been approved for public release and sale;  
its distribution is unlimited

**S** DTIC  
ELECTE  
NOV 10 1993  
**A**

93-27566



34pf

98

11

244



Submitted to: Surface Science

Date: 27 October 1993

Direct Images of Thermal Disorder in the Cl-Si and H-O-Si  
Chemisorption Bond on Si(100)

Q. Gao, Z. Dohnalek, C. C. Cheng<sup>††</sup>, W. J. Choyke<sup>†</sup> and J. T. Yates, Jr.

Surface Science Center  
Department of Chemistry  
University of Pittsburgh  
Pittsburgh, PA 15260

DTIC QUALITY INSPECTED 6

<sup>†</sup>Department of Physics  
University of Pittsburgh  
Pittsburgh, PA 15260

Accession For		
NTIS	CRA&I	<input checked="" type="checkbox"/>
DTIC	TAB	<input type="checkbox"/>
Unannounced		<input type="checkbox"/>
Justification		
By		
Distribution/		
Availability Codes		
Dist	Avail and/or Special	
A-1		

<sup>††</sup> Current address: AT&T Bell Laboratories  
600 Mountain Avenue  
Murray Hill, NJ 07974

Direct Images of Thermal Disorder in the Cl-Si and H-O-Si  
Chemisorption Bond on Si(100)

Q. Gao, Z. Dohnalek, C. C. Cheng, W. J. Choyke, and J. T. Yates, Jr.

Surface Science Center  
Department of Chemistry  
University of Pittsburgh  
Pittsburgh, PA 15260

**Abstract**

The electron stimulated desorption ion angular distribution (ESDIAD) technique combined with a digital subtraction method have been employed to generate difference ESDIAD patterns between measurements made at 130K and 305K for both adsorbed Cl and OH on Si(100). The difference ESDIAD patterns reveal, in real space, images of the thermally excited vibrational amplitudes of the adsorbates. This permits a qualitative visualization of the potential energy surface associated with an adsorbate on its adsorption site. For Cl/Si(100), isotropic thermal broadening of the Cl<sup>+</sup>-beams from 130K to 305K is observed. In contrast, OH/Si(100) exhibits anisotropic thermal broadening of the H<sup>+</sup>-beams on heating from 130K to 305K. These results are correlated with the vibrational frequencies of the surface oscillators.

**1. Introduction**

The vibrational dynamics of adsorbates are an important issue on surfaces since atomic motions are involved in the elementary steps for surface adsorption, surface diffusion and surface reaction processes. The investigation of adsorbate

vibrational motions on a well-characterized single crystal surface can provide detailed insights into the shape of the adsorbate-substrate interaction potential well. The shape of this potential well is significant in governing adsorption, surface diffusion, and surface reaction. For example, when a vibrational motion parallel to the surface is thermally excited to a large enough amplitude, i. e. passing the point of no-return on the potential energy surface, the adsorbate vibrational motion is then converted to lateral movement along the reaction coordinate for either surface diffusion or surface reaction.

ESDIAD [1,2] is a powerful technique for surface vibrational dynamics studies, complementary to laser-based spectroscopy methods [3]. The ESDIAD measurement has the advantage of directly imaging the thermal disorder in surface chemical bond directions, giving information about adsorbate vibrational motions in real space. In contrast, vibrational spectroscopic methods indirectly reflect the vibrational movements in the frequency domain.

When an adsorbate-substrate system is subjected to excitation by an electron beam, the electronically excited adsorbate ejects molecular or atomic fragments (ions or neutrals) from the surface, along a direction nearly parallel to the direction of the chemical bond being broken. Since the electronic transition is much faster ( $\sim 10^{-15}$  sec) than the nuclear motion (Franck-Condon transition process), the spatially recorded ESDIAD pattern is a superposition of sub-picosecond snapshots of the instantaneous bond direction of the adsorbate, averaged over many identical adsorbed species undergoing their zero-point and thermal motions. Therefore, ESDIAD provides a statistical picture of the distribution of bond directions at a particular surface temperature.

Clinton[4] has indicated, from the quantum scattering analysis of the Franck-Condon desorption cross-section, that the maximum in the ESDIAD patterns corresponds to the average bond direction; the peak shape is a reflection

of the probability density function of the components of vibrational motion parallel to the surface. At a given temperature,  $T$ , the thermally averaged contributions of all the  $n$ th vibrational states,  $\psi_n(\alpha)$ , will give an angularly dependent electron stimulated desorption (ESD) cross section,  $\sigma(\alpha)$ , at desorption angle  $\alpha$  as follows (with non-degenerate vibrational normal modes) [5]:

$$\sigma(\alpha) \sim \sum_{n=0}^{\infty} |\psi_{n(\alpha)}|^2 P_{(n)} \quad (1)$$

where  $\psi_n(\alpha)$  is the vibrational wave function, and  $P_{(n)}$  is the Boltzmann statistical weighting factor. Each individual vibrational state,  $\psi_n(\alpha)$ , contributes to the total population of the vibrational states at temperature  $T$  with a statistical weighting factor of:

$$P_{(n)} = \frac{\exp [-(E_n - E_0) / kT]}{\sum_{n=0}^{\infty} \exp [-(E_n - E_0) / kT]} \quad (2)$$

Here,  $(E_n - E_0)$  is the energy difference between an upper state and the ground state vibrational levels.

In this report, we employ an ESDIAD pattern analysis procedure involving the subtraction of a low temperature-ESDIAD pattern from a high temperature-ESDIAD pattern. The difference pattern provides information about the extra vibrational amplitude excited at high temperature. A clear view is presented in real space of the vibrational excursions of the adsorbate in various azimuthal directions by thermal excitation. This information is not available from spectroscopic methods. We show an anisotropic thermal broadening of

OH/Si(100) in contrast to an isotropic thermal broadening of Cl/Si(100), consistent with known structural and vibrational properties of the two systems.

The Si(100) substrate provides highly directional covalent bonds at its surface, and is, therefore, a logical candidate for the study of the isotropy of thermal broadening of surface bond directions by ESDIAD. It is well known that the Si(100) surface reconstructs forming a (2x1) structure from the dimerization of the surface atoms [6]. The reconstructed surface consists of parallel rows of Si<sub>2</sub> dimers. Each surface Si atom has one inclined dangling bond pointed outward from the surface which can bind to the incoming adsorbate. The slight deviation from the <100> direction after cutting a Si crystal results in a real Si(100) surface with wide adjacent terraces separated by monatomic height steps, exhibiting orthogonal Si<sub>2</sub> dimer domains of (2x1) and (1x2) structure[7].

The chemisorption of Cl<sub>2</sub> on Si(100) leads to dissociation [8,9]. At saturation, each Si<sub>2</sub> dimer is capped with two Cl atoms, one Cl on each dangling bond inclined  $25^\circ \pm 4^\circ$  from the normal [8,9]. Previous studies have shown that this is the stable Cl/Si(100) structure produced by heating a metastable Cl layer with a different structure to 673K [8,9]. The bonding structure and the vibrational normal modes of Cl/Si(100) are shown in fig. 1. Comparing the frequencies of the Si-Cl in-plane bending ( $180\text{-}254\text{ cm}^{-1}$ ) [10,11] and out-of-plane bending ( $\sim 200\text{ cm}^{-1}$ ) [11] modes, one expects a nearly isotropic thermal broadening of the Cl<sup>+</sup> ESDIAD beams if the bending vibrations dominate the broadening process as previously reported [12].

The adsorption of H<sub>2</sub>O on Si(100) at room temperature is also dissociative [13-17]. The bonding configuration for a surface OH group is presented in fig. 2, together with the approximate vibrational normal mode frequencies associated with it [18-20]. The large difference in frequency of the SiOH bending mode ( $\sim 1070\text{ cm}^{-1}$ ) and the SiOH torsional mode ( $\sim 200\text{ cm}^{-1}$ ) [18-20] is consistent with

anisotropic thermal broadening of the OH bond directions, since the  $\sim 200 \text{ cm}^{-1}$  mode will undergo extensive thermal excitation.

The stretching vibrations of Si-Cl and O-H bonds are of minor importance for the thermally induced broadening observed in ESDIAD because of their relatively high energy spacings. Thermal excitation of these modes will be insignificant at the temperatures employed here.

## 2. Experimental

The ultrahigh vacuum (UHV) system has a base pressure of  $\sim 3 \times 10^{-11}$  torr. It is equipped with a digital ESDIAD/LEED apparatus, a cylindrical mirror analyzer (CMA) Auger electron spectrometer (AES), an ion sputtering gun, a shielded quadrupole mass spectrometer (QMS) for line-of-sight temperature programmed desorption (TPD) studies, and an additional QMS with an electron gun and grid lenses for ion mass analysis during electron stimulated desorption (ESD). A detailed description of the UHV system and Si(100) crystal preparation can be found elsewhere [21,22]. A multi-capillary-collimated doser was used for  $\text{Cl}_2$  and  $\text{H}_2\text{O}$  introduction [23-25].

Mass spectrometric studies of the ions produced during ESD indicate that  $\text{Cl}^+$  ions (for the Cl/Si(100) system) [8,9] and  $\text{H}^+$  ions (for the OH/Si(100) system) are the species contributing to the observed ESDIAD pattern [26].

The electron beam energy used for ESDIAD studies is 120 eV. The electron beam current, measured between the crystal and ground (uncorrected for the secondary electrons), is very small ( $\sim 5 \text{ nA}$ ), thus limiting beam-induced surface damage during data collection. Due to the finite detection solid angle of the ESDIAD apparatus, a positive bias is supplied to the crystal to compress the ion trajectories. This compression voltage is +10.0 V for the Cl/Si(100) system and

+100 V for the OH/Si(100) system. The compression of ion trajectories does not affect the qualitative interpretation presented here. For all the ESDIAD measurements, the crystal is not heated by an electrical current, avoiding electrical effects on the ESDIAD pattern.

The ESDIAD patterns at different temperatures, and after the digital subtraction, have been azimuthally smoothed to remove the slight inhomogeneities of the ion optics and/or the MCP detector [27]. The smoothing method is based on the symmetry of the observed ESDIAD pattern and the assumption that ion intensities  $180^\circ$  apart in the azimuthal angle should be equal due to the two-fold symmetry of the Si(100)-(2x1) and (1x2) domains. To improve the signal-to-noise in the difference patterns, long data collection times were employed involving the collection of  $\sim 10^7$  ions/pattern.

The cleanliness and structure of the Si (100)-(2x1) surface have been checked by AES and digital LEED for each adsorption cycle. AES indicates a clean surface with C(KLL):Si(LMM), O(KLL):Si(LMM), and Cl(LMM):Si(LMM) AES peak-to-peak intensity ratios  $<1 \times 10^{-3}$ .

### 3. Results

#### 3.1 Thermal Broadening of ESDIAD Patterns For Cl/Si(100) and OH/Si(100)

Two off-normal  $\text{Cl}^+$  ion beams are produced for Cl atoms bound to a symmetric  $\text{Si}_2$  dimer site (fig. 1) during ESD process. The probing of both (2x1) and (1x2) orthogonal domains by the incident electron beam generates four  $\text{Cl}^+$  ion beams corresponding to four off-center peaks in the ESDIAD pattern. Figure 3a is a  $\text{Cl}^+$ -ESDIAD pattern at 130K. Figure 3b shows an ESDIAD pattern

obtained after warming up to 305K with all other conditions for data collection held constant. The broadened individual peak profiles at the elevated temperature may be seen in the perspective plot (fig. 3b). If the sample is cooled back down to 130K, the low temperature ESDIAD pattern (fig. 3a) is reproduced, indicating a reversible thermal process. No chemical reaction is observed in this temperature range [8,9].

Reversible thermal broadening of the  $H^+$  ion beams is also observed for OH/Si(100). The OH group adsorbed on the dangling bond of a  $Si_2$  dimer (fig. 2) will produce an off-normal  $H^+$  ion beam during the ESD process, and the (2x1) and (1x2) domains of Si(100) will therefore yield four  $H^+$  ion beams. The 130K-ESDIAD pattern of  $H^+$  ion beams from OH(a) is shown in fig. 4a and the broadened  $H^+$  pattern at 305K is shown in fig. 4b. No chemical reaction is observed in this temperature range [16,17].

### 3.2 The Difference ESDIAD Pattern For Cl/Si(100)

While the temperature dependent ESDIAD patterns of Cl/Si(100) and OH/Si(100) appear to be similar (fig. 3 and fig. 4), the difference patterns shown in fig. 5 and 6 are quite dissimilar and reveal the different dynamical behavior of Cl/Si(100) compared to OH/Si(100).

Fig. 5a results from the subtraction of the 130K- $Cl^+$  ESDIAD pattern (fig. 3a) from the 305K ESDIAD pattern (fig. 3b). The total ion signal difference pattern presented in fig. 5a contains on the order of  $10^6$   $Cl^+$  counts for the positive contribution matched by negative contribution of the same magnitude. The outside boundary regions in the difference pattern are nearly zero in intensity, and provide a secondary reference level for identifying the positive and negative features of the difference pattern (fig. 5a). The  $Cl^+$  difference pattern (fig. 5a) has two features:

- (1) The intensity gain at 305K, corresponding to the positive intensity regions after subtraction, are found in a strong normal peak at the center of the difference pattern, and in four smaller ridges of positive intensity along the diagonal directions ( $\langle 010 \rangle$  and  $\langle 0\bar{1}0 \rangle$  azimuths) two of which are centered on section A.
- (2) The intensity losses at 305K, corresponding to the negative intensity regions in fig. 5a, are found approximately at the  $\text{Cl}^+$  peak positions observed before subtraction (fig. 3). Two of these regions are centered on section B. The procedures used for generating the model ESDIAD difference pattern shown in fig. 5b will be discussed later.

### 3.3 The Difference ESDIAD Pattern For OH/Si(100)

In contrast to the difference pattern for  $\text{Cl}/\text{Si}(100)$  (fig. 5a), the difference pattern for  $\text{OH}/\text{Si}(100)$  (fig. 6a) does not show a prominent intensity gain in the central region at 305K. Instead, positive differences are observed along ridges off-center in diagonal directions on the contour plot (fig. 6a). Section A contains two of the four ridge regions. The ion signal presented in fig. 6a has positive contribution of  $\sim 10^6 \text{ H}^+$  ion counts and a negative contribution of the same magnitude. The region of negative contribution is located approximately at the  $\text{H}^+$  peak positions in the original ESDIAD patterns (fig. 4). Two of these negative regions are located along section B. The procedures used to produce the model ESDIAD difference pattern shown in fig. 6b will be described later.

## 4. Discussion

### 4.1 Bond Vibration And Thermal Broadening

The solid lines in fig. 7 give a cross sectional cut through the difference pattern for Cl/Si(100) along directions A and B ( $\langle 010 \rangle$  and  $\langle 011 \rangle$  azimuths) in fig. 5a. Section A in fig. 7 shows that the central region contains most of the intensity gain at 305K. There is also an intensity gain seen in shoulders on the central peak. Since the thermally excited in-plane bending mode of the Si-Cl bond (fig. 1b) broadens the  $\text{Cl}^+$  ion beam, four such broadened beams overlap in the center region. In addition, the smaller intensity gain in the diagonal directions ( $\langle 010 \rangle$  and  $\langle 0\bar{1}0 \rangle$  azimuths) of the contour plot (fig. 5a) gives four off-center ridges, and two of them are shown as shoulders in section A (fig. 7). These ridges are due to the thermal excitation of the Si-Cl out-of-plane bending mode (fig. 1c), which broadens the  $\text{Cl}^+$  beam in directions perpendicular to the Cl-Si-Si plane; peak overlap from the different Si-Cl bonds occurs here in the diagonal directions.

Section B displays, besides the intensity gain in the central region of the pattern, the intensity loss in the original Si-Cl equilibrium bond directions. The thermal excitation of both the in-plane and out-of-plane bending modes of the Si-Cl bond (fig. 1b-c) from the ground state into higher energy levels at 305K leads to the Si-Cl bond having lower probability of being found in its equilibrium position; this yields a negative difference in  $\text{Cl}^+$  intensity near this position.

The solid lines in fig. 8 show the detailed cross section analysis of the difference pattern for OH/Si(100) along directions A and B ( $\langle 010 \rangle$  and  $\langle 011 \rangle$ ) in fig. 6a. Section A shows that positive intensity is contributed primarily by overlapping features which are located off normal along the  $\langle 010 \rangle$  direction. The positive features in Section A are due to the thermal excitation of the Si-OH

torsional mode (fig. 2c) into upper energy levels. The excited torsional mode broadens the  $H^+$  ion beam in directions perpendicular to the H-O-Si plane. The overlap of the four broadened  $H^+$ -beams from orthogonal domains occurs in the diagonal region producing ridges in the difference pattern ( as shown in the perspective plot in fig.6). Section B in fig. 8 shows that the intensity loss at 305K is near the original  $H^+$  peak positions (fig. 4). The same argument made for the intensity loss of Cl/Si(100) at 305K applies for the OH/Si(100). Since the thermal excitation of the SiOH torsional mode into upper levels depopulates the ground state, the OH bond has a lower probability of being found at its equilibrium bond direction, leading to a reduction of  $H^+$ -beam intensity in this direction at 305K. The origin of the model curve will be discussed later.

#### 4.2 Thermal Population of the Vibrational Energy Levels

The qualitative interpretation discussed above (section 4.1) is supported by the following quantitative analysis. Using the harmonic oscillator approximation,  $(E_n - E_0) = nh\nu$ , the statistical weighting factor for the  $n$ th vibrational state in equation (2) is:

$$P_{(n)} = [\exp(-nh\nu) / kT][1 - \exp(-h\nu / kT)] \quad (3)$$

For the two substrate temperatures employed in the experiments, 130K and 305K, the population for each state at each temperature can be calculated from equation (3) using the estimated vibrational frequencies. Table 1 summarizes the population of the vibrational state for the Si-Cl and Si-OH normal modes. The stretching vibrations for the Si-Cl and the O-H bonds are neglected due to their minor relevance to the thermal broadening.

For the Cl/Si(100) system, the following conclusions are evident from analyzing the population of each vibrational state as a function of the substrate temperature: (1) There is a substantial depopulation ( $\Delta P(n=0) \sim 28\%$ ) of the ground state for both in-plane and out-of-plane bending modes of the Si-Cl bond at 305K compared to 130K. The depopulation will lead to an intensity loss upon heating in the equilibrium Si-Cl bond direction as observed in the difference pattern (fig. 5a); (2) At 305K, the  $n \geq 1$  vibrational states for both the in-plane and out-of-plane Si-Cl bending modes are considerably populated as shown in Table 1. The population of upper states will result in a larger vibrational amplitude in the directions associated with these modes, as discussed later (section 4.3); (3) Isotropic broadening of the Si-Cl pattern is expected based on the presence of in-plane and out-of-plane vibrational modes of similar frequency ( $\sim 200 \text{ cm}^{-1}$ ).

Different vibrational dynamics are expected for the SiOH bond. (1) The large energy for excitation of the SiOH bending mode,  $\sim 1070 \text{ cm}^{-1}$  [18-20], leads to little excitation of the SiOH bending mode over the 130K to 305K temperature range. (Table 1). Therefore, the broadening in the azimuthal direction corresponding to the H-O-Si plane (fig.2) is expected to be small for the temperature range studied here (130K - 305K); (2) The SiOH torsional mode will be the major contributor to shape changes in the  $\text{H}^+$  ESDIAD pattern on raising the temperature because of its low frequency; (3) The factors mentioned in (1) and (2) will result in an anisotropic thermal broadening effect.

#### 4.3 Mean Square Amplitude of Normal Modes

The mean square amplitude of an oscillator is directly related to its quantum state specified by the quantum number,  $n$ , within the harmonic oscillator approximation. Using the normal coordinate,  $Q = m^{1/2} x$ , as discussed by Wilson, Decius and Cross [28], with  $x$  as the displacement and  $m$  as the mass, the mean

value of an observable (the square amplitude,  $\langle Q^2 \rangle$ , in this case) in its quantum state,  $\psi_n(Q)$ , can be evaluated as [29,30]:

$$\langle Q_n^2 \rangle = \langle \psi_{n(Q)} | Q^2 | \psi_{n(Q)} \rangle = \frac{\hbar}{4\pi^2 c \nu} \left( n + \frac{1}{2} \right) \quad (4)$$

in which  $\nu$  is the wavenumber of the normal mode and  $c$  is the speed of light.

From eqn. (4), the mean square amplitude for a given normal mode is expected to increase linearly with the quantum number,  $n$ . Furthermore, it is evident, from eqn. (4), that a low frequency oscillator will have a larger mean square amplitude than a high frequency one.

#### 4.4 Modeling of The ESDIAD Patterns For Cl/Si(100) and OH/Si(100)

Both Cl/Si(100) and OH/Si(100) systems have been modeled for the vibrational behavior of the Si-Cl and SiOH bonds. In the modeling of Cl/Si(100), the following optimized parameters have been employed for the 305K ESDIAD pattern compared to the 130K ESDIAD pattern using a Gaussian distribution for the individual ion beams profiles: (1) an isotropic 20% increase in full width at half maximum (FWHM) of the Gaussian distribution; (2) a 10% increase in the integrated ion yield corresponding to that measured experimentally; (3) a 5% decrease in the apparent  $\text{Cl}^+$  ion polar angle detected, which is not explored further here. The modeled difference pattern (fig. 5b; fig. 7 with dashed lines) agrees quite well with the experimental results (fig. 5a; fig. 7 with solid lines).

For the OH/Si(100) system, the following parameters are used for modeling the ESDIAD pattern at 305K compared to 130K: (1) a 2% increase of the FWHM of the  $\text{H}^+$  beam Gaussian distribution in the  $\text{Si}_2$  dimer bond azimuthal direction component (in O-Si-Si plane). In contrast, an 8% increase of the FWHM is employed for the orthogonal azimuthal direction component; (2) an increase in the

integrated volume of the Gaussian peak profiles of  $\sim 3\%$ , in accordance with the total  $H^+$  ion yield measured experimentally; and (3) a small decrease ( $\sim 6\%$ ) in polar angle for the  $H^+$  beams, for which the origin is not explored here. The modeled difference pattern (fig. 6b; fig. 8 with dashed lines) also agrees well with the experimental results (fig. 6a; fig. 8 with solid lines). Thus in this case the anisotropy for the two -OH modes is approximately a factor of four.

It is not appropriate in the analysis to quantitatively estimate  $\langle Q_n^2 \rangle$  from the ESDIAD data presented here, since the laboratory angles measured depend upon crystal bias and ion energy and therefore possess a complex relationship to  $\langle Q_n^2 \rangle$ .

The above analysis of the vibrational dynamics of the adsorbates has qualitatively explained the observed isotropic and anisotropic thermal broadening processes. However, it should be kept in mind that there are additional factors to be evaluated for a full interpretation of the results, such as the beam broadening caused by the retention of the momentum of the initial state by the departing ion of the adsorbates [5, 31], and the perturbations of the departing ion motions (final state effect). Two prominent final state effects are: (1) Ion trajectory distortion toward the surface by an electrostatic image potential (a long range effect); and (2) Ion trajectory distortion away from the surface due to preferential neutralization of the desorbing ions in the near surface region (a short range effect). These two effects have been studied in detail elsewhere [8, 32-33].

## 5. Conclusion

The ESDIAD method is shown to be a high resolution technique for study of adsorbate vibrational dynamics. By employing ESDIAD pattern subtraction methods, the thermal disorder in chemical bond directions on the surface may be

mapped, giving a qualitative insight into of the potential energy surface for an adsorbate near its equilibrium bonding position. Examples of isotropic vibration ( $Cl/Si(100)$ ) and anisotropic vibration ( $OH/Si(100)$ ) are presented and the relation to the estimated normal mode frequencies has been established.

## 6. Acknowledgments

We would like to thank the Office of Naval Research for support of this work. We thank R. D. Ramsier for a careful reading of the manuscript.

## References

1. J. T. Yates, Jr., M. D. Alvey, M. J. Dresser, M. A. Henderson, M. Kiskinova, R. D. Ramsier, A. Szabo, *Science* 255 (1992)1397, and references therein.
2. R. D. Ramsier and J. T. Yates, Jr., *Surf. Sci. Rep.*, 12 (1991) 243, and references therein.
3. For a recent review, see R. R. Cavanagh, D. S. King and J. C. Stephenson, *J. Phys. Chem.* 97 (1993) 786.
4. W. L. Clinton, *Phys. Rev. Lett.* 39 (1977) 965.
5. W. Riedl and D. Menzel, *Surf. Sci.* 207 (1989) 494.
6. R. E. Schlier and H. E. Farnsworth, *J. Chem. Phys.* 30 (1959) 4; (b) R. M. Tromp, R. J. Hamers, and J. E. Demuth, *Phys. Rev.* B34 (1986) 5343.
7. F. K. Men, W. E. Packard, and M. B. Webb, *Phys. Rev. Lett.* 61 (1988) 2469.
8. Q. Gao, C. C. Cheng, P. J. Chen, W. J. Choyke and J. T. Yates, Jr., *J. Chem. Phys.* 98 (1993) 8308.
9. C.C. Cheng, Q. Gao, W. J. Choyke and J. T. Yates, Jr., *Phys. Rev.* B46 (1992) 12810.
10. A. L Smith, *J. Chem. Phys.* 21 (1953) 1997.
11. J. R. Durig, C. W. Hawley, *J. Chem. Phys.* 58 (1973) 237.
12. C. C. Cheng, Q. Gao, Z. Dohnalek, W. J. Choyke, and J. T. Yates, Jr., *J. Chem. Phys.*, in press.
13. F. Stucki, J. Anderson and G. J. Lapeyre, *Surf. Sci.* 143 (1984) 84.
14. H. Ibach, H. Wagner and D. Bruchmann, *Solid State Commun.* 42 (1982) 457.
15. Y. J. Chabal, *Phys. Rev.* B29 (1984) 3677.

- 16 Z. Dohnalek, Q. Gao, C. C. Cheng, W. J. Choyke, and J. T. Yates, Jr., in preparation.
- 17 C.U.S. Larson, A.L. Johnson, A. Hodstrom, T.E. Madey, *J. Vac. Sci. Technol.*, A8 (1987) 842.
- 18 J. Rouviere, V. Tabacik and G. Fleury, *Spectrochim. Acta Part A* 29 (1973) 229.
- 19 V. K. Licht and H. Krigsmann, *Z. Anorg. Alleg. Chem.* 323 (1963) 190.
- 20 E. J. Heilweil, M. P. Casassa, R. R. Cavanagh and J. C. Stephenson, *J. Chem. Phys.* 85 (1986) 5004.
- 21 R.M. Wallace, P.A. Taylor, W.J. Choyke and J.T. Yates, Jr., *Surf. Sci.* 239 (1990) 1.
- 22 R.M. Wallace, C.C. Cheng, P.A. Taylor, W.J. Choyke and J.T. Yates, Jr., *Appl. Surf. Sci.*, 45 (1990) 20.
- 23 M.J. Bozack, L. Muehlhoff, J.N. Russell, Jr., W.J. Choyke and J.T. Yates, Jr., *J. Vac. Sci. Technol.*, A5 (1987) 1.
- 24 A. Winkler and J. T. Yates, Jr., *J. Vac. Sci. Technol.* A6 (1988) 2929;
- 25 C. T. Campbell, S. M. Valone, *J. Vac. Sci. Technol.*, A3 (1985) 408.
- 26 Our ESDIAD studies of the monohydride phase on Si(100) confirm that the  $H^+$  ion in the  $H_2O/Si(100)$  system is from the OH group instead of from the Si-H group, in agreement with the result of ref. 17.
- 27 A. Szabo, M. Kiskinova, and J. T. Yates, Jr., *Surf. Sci.*, 205 (1988) 207.
- 28 E. B. Wilson, Jr., J. C. Decius and P. C. Cross, *Molecular Vibrations*, McGraw-Hill Book Company, Inc., New York, 1955, p.17.
- 29 S. R. Hemley, N. Ostrowsky and S. Ostrowsky, *Quantum Mechanics*, Vol. 1, Hermann and John Wiley & Sons, Inc., New York, 1977, p.227.
- 30 S. J. Cyvin, *Molecular Vibrations and Mean Square Amplitudes*, American Elsevier Publishing Company Inc., New York, 1968, p.76.

31. A. Szabo and J. T. Yates, Jr., *J. Chem. Phys.*, 98 (1993) 689.
32. M. Nishijima and F. M. Propst, *Phys. Rev. B2* (1970) 2368; Z. Miskovic, J. Vukanic and T. E. Madey, *Surf. Sci.* 169 (1986) 405.
33. Z. Miskovic, J. Vukanic and T. E. Madey, *Surf. Sci.* 141 (1984) 285.

### Figure Captions

- Fig. 1.** Configuration and normal modes of terminally bonded Cl atoms adsorbed on a symmetric Si<sub>2</sub> dimer site on Si(100).
- Fig. 2.** Surface species resulting from H<sub>2</sub>O dissociative adsorption on Si(100) with the OH on one dangling bond of the symmetric Si<sub>2</sub> dimer and the H atom on the other.
- Fig. 3.** Reversible temperature dependent ESDIAD patterns of Cl/Si(100). (a) 130K Si substrate temperature; (b) 305 K Si substrate temperature. The figures on the left are perspective plots; they are generated by mapping the counts of Cl<sup>+</sup> ions in the z direction as a function of the (x,y) coordinates on the detector. The figures on the right are contour plots. Each contour line in each individual plot represents an increment of 1/7 of the maximum count rate at a peak, with a width of ±5% of the median value of that contour.
- Fig. 4.** Reversible temperature dependent ESDIAD patterns of OH/Si(100). (a) 130K Si substrate temperature; (b) 305 K Si substrate temperature. H<sub>2</sub>O was adsorbed at 305K to saturation. The figures on the left are perspective plots; they are generated by mapping the counts of H<sup>+</sup> ion of the adsorbed OH group in the z direction as a function of the (x,y) coordinates on the detector. The figures on the right are contour plots. Each contour line in each individual plot represents an increment of 1/7 of the maximum count rate at a peak, with a width of ±5% of the median value of that contour.

**Fig. 5.** The difference ESDIAD patterns for Cl/Si(100). (a) Experimental difference pattern obtained by digital subtraction of 130K ESDIAD pattern (fig. 3a) from 305 K ESDIAD pattern (fig. 3b). (b) Modeled difference ESDIAD pattern with Gaussian distribution peak profiles.

**Fig. 6.** The difference ESDIAD patterns for OH/Si(100). (a) Experimental difference pattern obtained by digital subtraction of 130K ESDIAD pattern (fig. 4a) from 305 K ESDIAD pattern (fig. 4b). (b) Modeled difference ESDIAD pattern with Gaussian distribution peak profiles.

**Fig. 7.** Cross section views of the difference ESDIAD pattern of Cl/Si(100) shown in fig. 5 cut in directions A and B. Solid lines represent the experimental data while the dashed lines show model calculations involving isotropic broadening of the four Cl<sup>+</sup> ESDIAD beams. The angles presented in the figure are the measured angles without correction for ion trajectory and final state effects.

**Fig. 8.** Cross section views of the difference ESDIAD pattern of OH/Si(100) shown in fig. 6 cut in directions A and B. Solid lines represent the experimental data while the dashed lines show model calculations involving anisotropic broadening of the four H<sup>+</sup> ESDIAD beams. The angles presented in the figure are the apparent angles without correction for ion trajectory and final state effects.

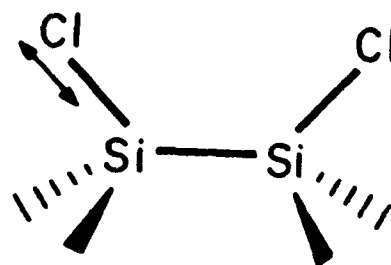
Table. 1 The population of the vibrational energy levels at 130K and 305K for Cl/Si(100) and OH/Si(100)

Calculation is made with approximate frequencies estimated from references 10-11, 18-20.

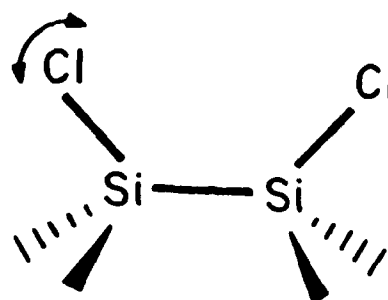
$\nu$ ( $\text{cm}^{-1}$ )	$P_{(n=0)}$ (%)		$P_{(n=1)}$ (%)		$P_{(n=2)}$ (%)		$P_{(n=3)}$ (%)		
	130K	305K	130K	305K	130K	305K	130K	305K	
Si-Cl in-plane bending	~ 200	89.1	61.1	9.7	23.8	1.1	9.2	0.1	3.6
Si-Cl out-of-plane bending	~ 200	89.1	61.1	9.7	23.8	1.1	9.2	0.1	3.6
SiOH torsion	~ 200	89.1	61.1	9.7	23.8	1.1	9.2	0.1	3.6
SiOH bending	~ 1070	100	99.4	0	0.6	0	0	0	0

# Schematic of The Normal Modes of Cl on Si(100)-(2x1)

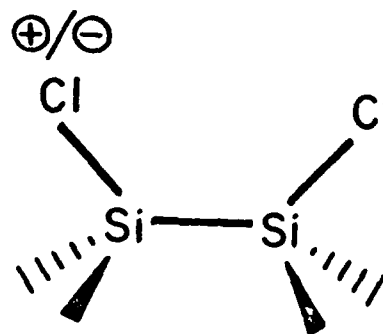
(a) stretching  
550 - 600  $\text{cm}^{-1}$



(b) in plane bending  
 $\sim 200 \text{ cm}^{-1}$

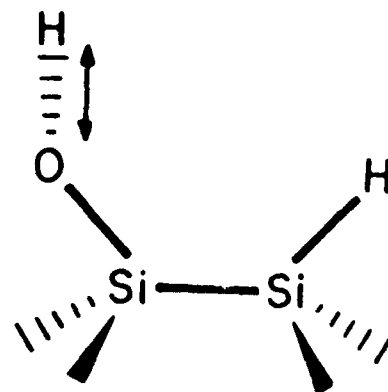


(c) out-of-plane bending  
 $\sim 200 \text{ cm}^{-1}$

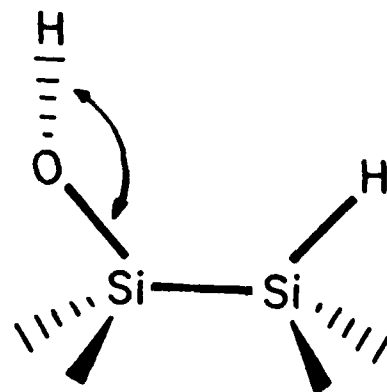


# Schematic of The Normal Modes of OH on Si(100)-(2x1)

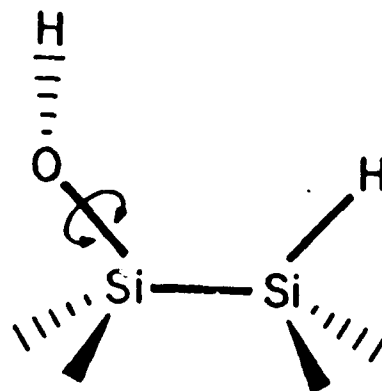
(a) OH stretching  
 $\sim 3690 \text{ cm}^{-1}$



(b) SiOH bending  
 $\sim 1070 \text{ cm}^{-1}$

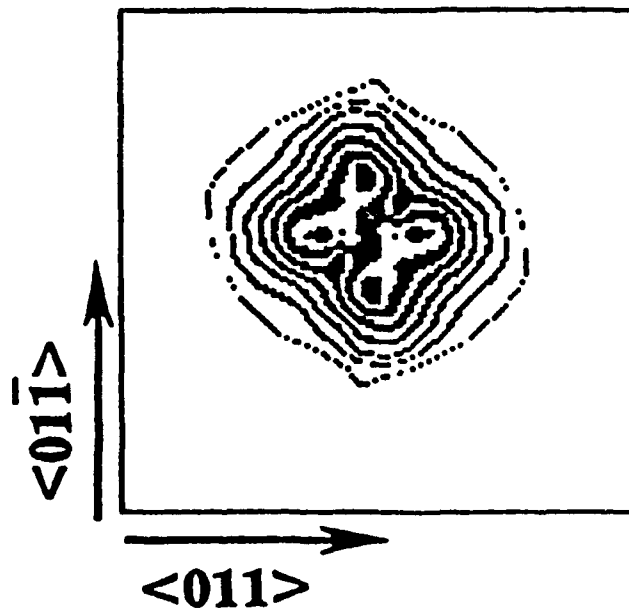


(c) SiOH torsion  
 $\sim 200 \text{ cm}^{-1}$

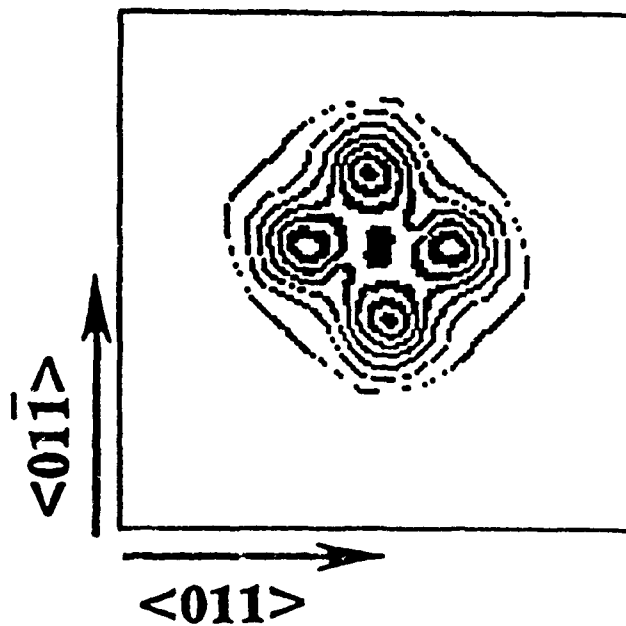
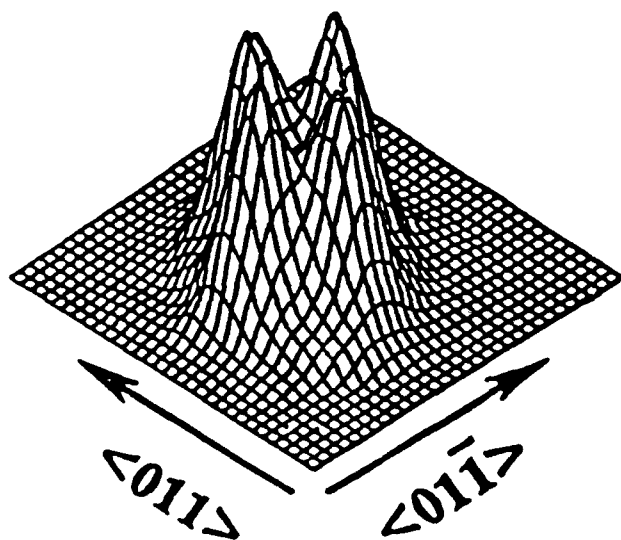


# ESDIAD Patterns of Cl on Si(100)

(b)  $T_{\text{crystal}} = 305 \text{ K}$

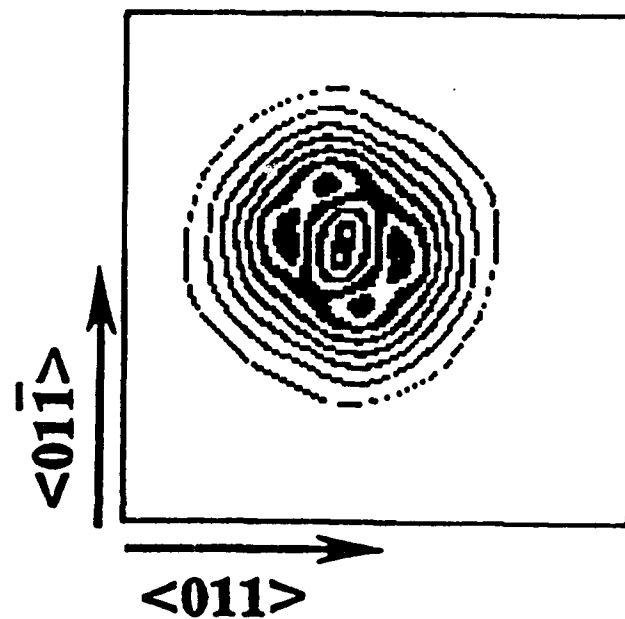
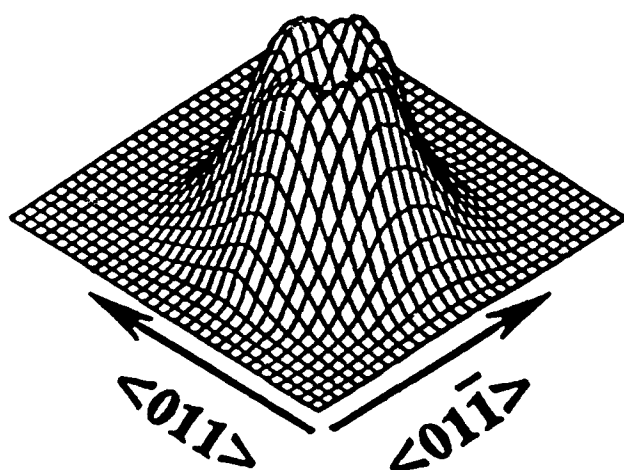


(a)  $T_{\text{crystal}} = 130 \text{ K}$

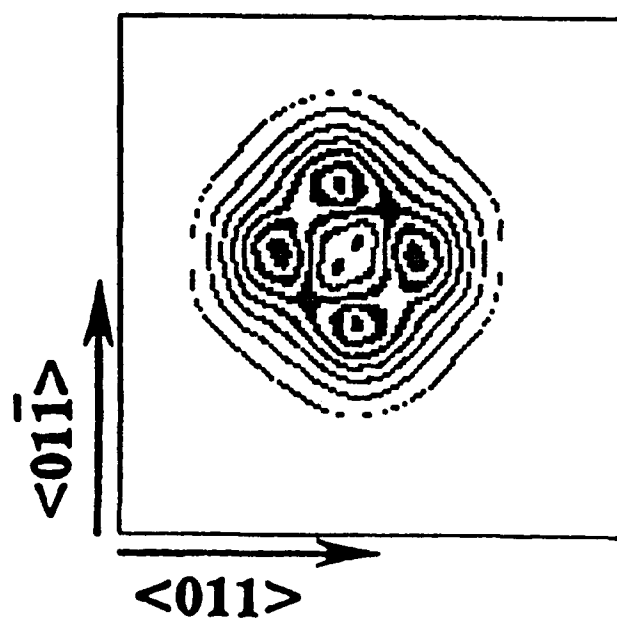


# ESDIAD Patterns of OH on Si(100)

(b)  $T_{\text{crystal}} = 305 \text{ K}$

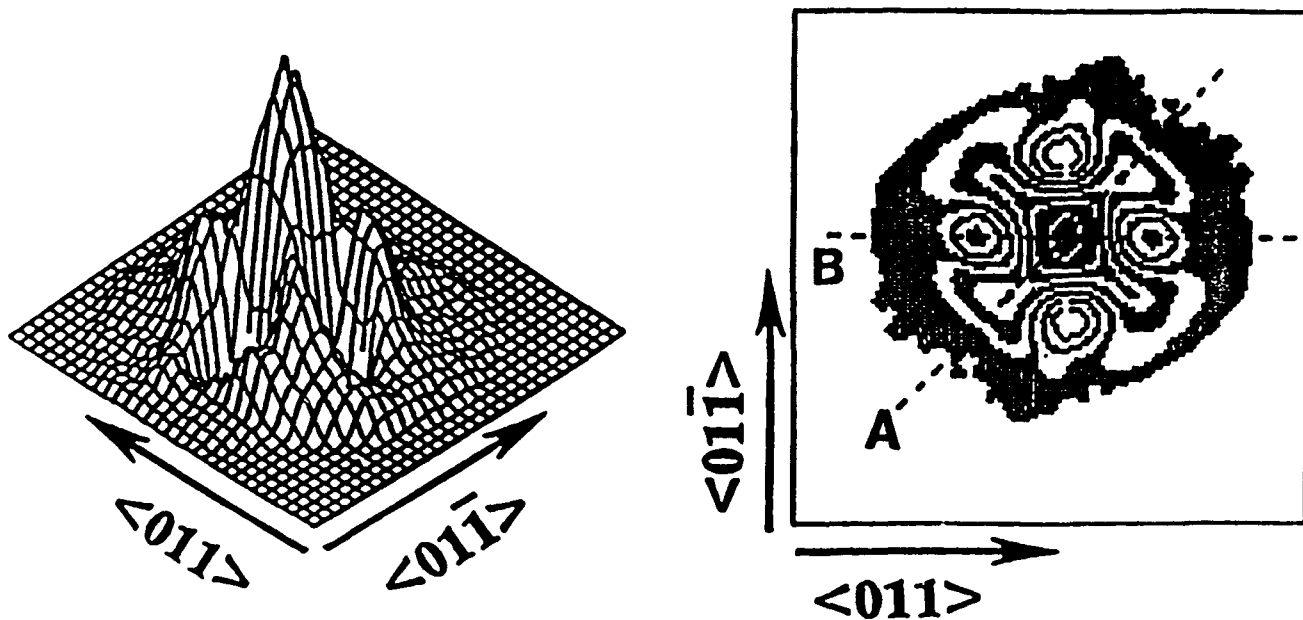


(a)  $T_{\text{crystal}} = 130 \text{ K}$

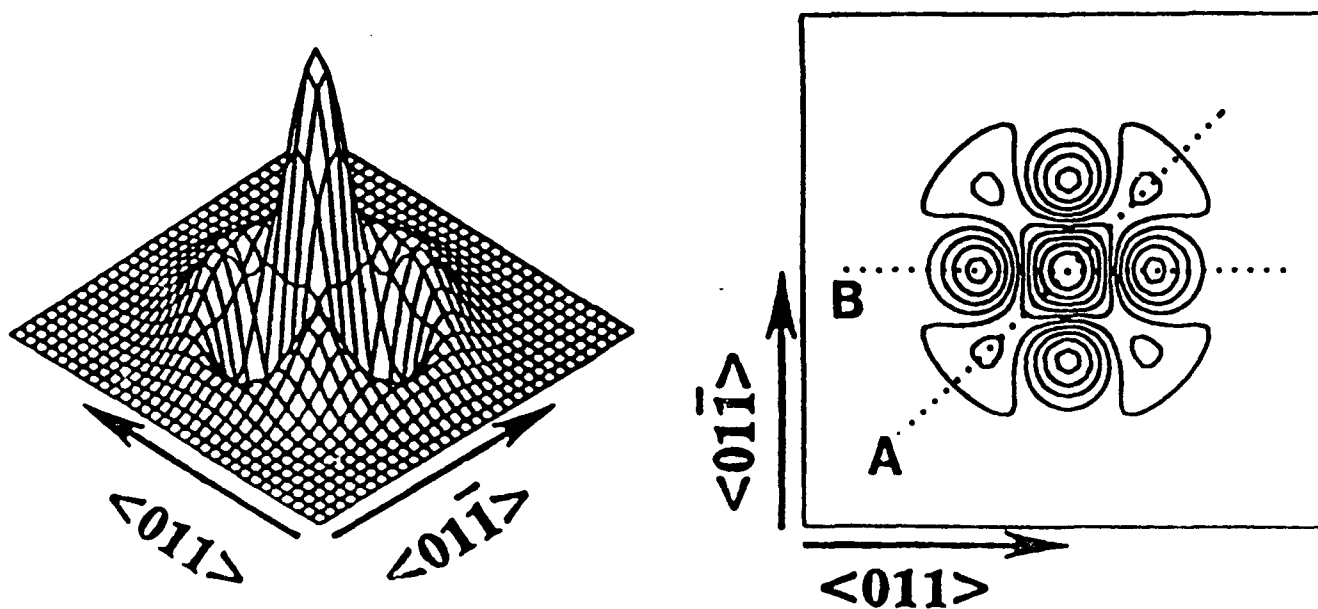


# Difference ESDIAD Patterns of Cl/Si(100)

## (a) Experimental

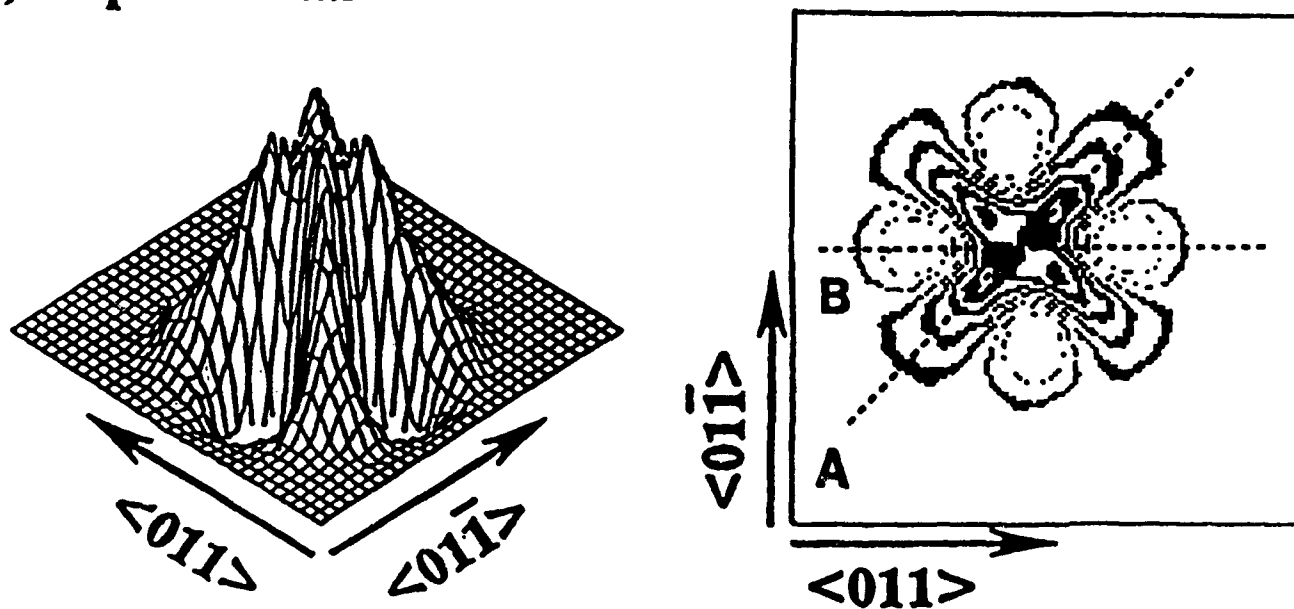


## (b) Model

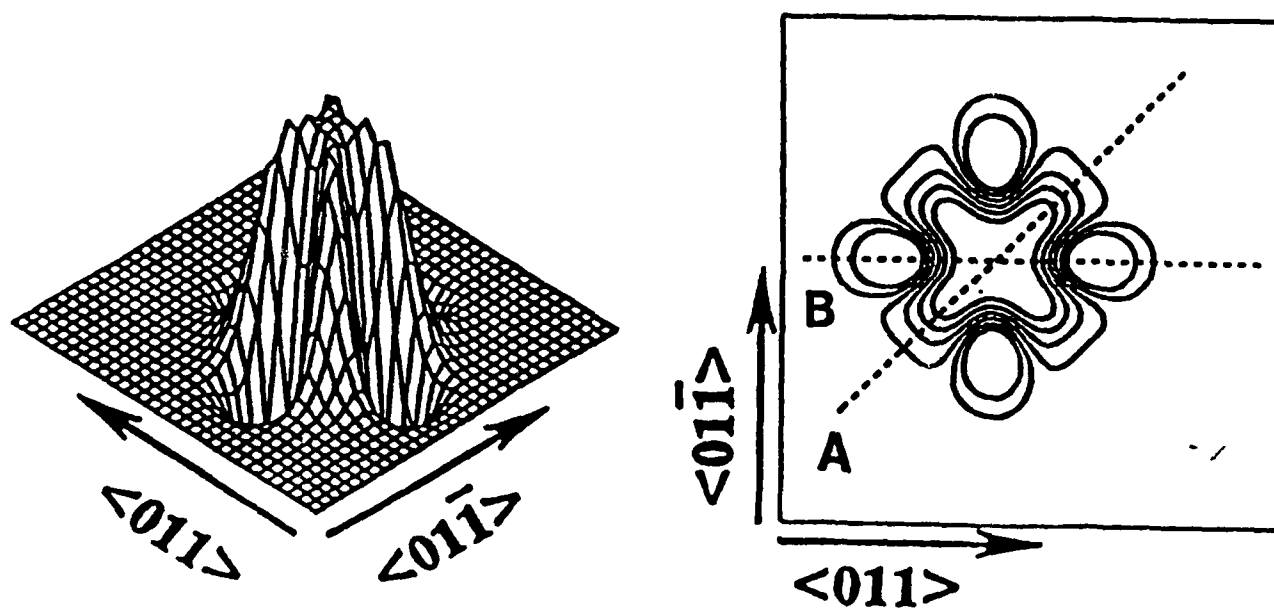


# Difference ESDIAD Patterns of OH/Si(100)

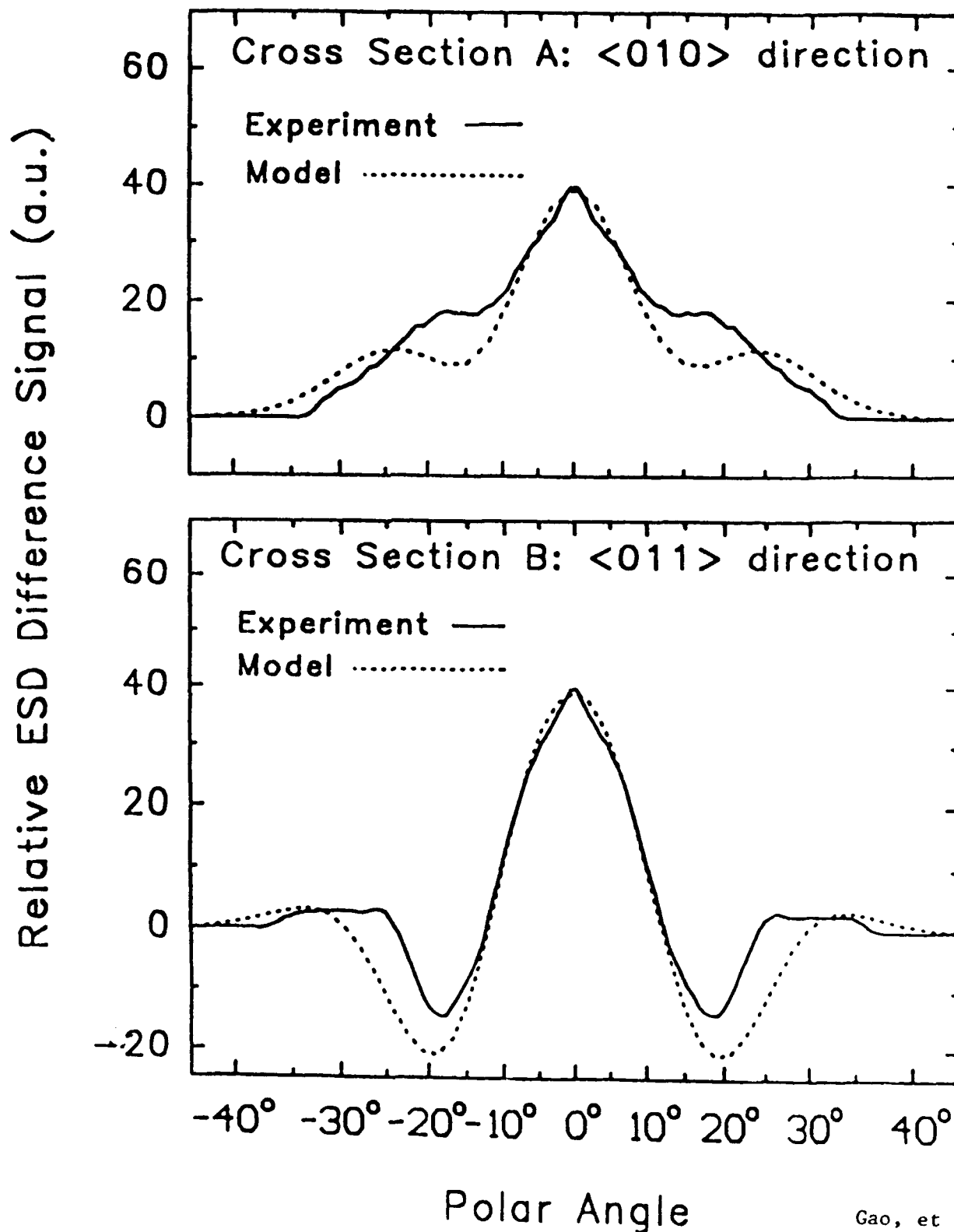
## (a) Experimental



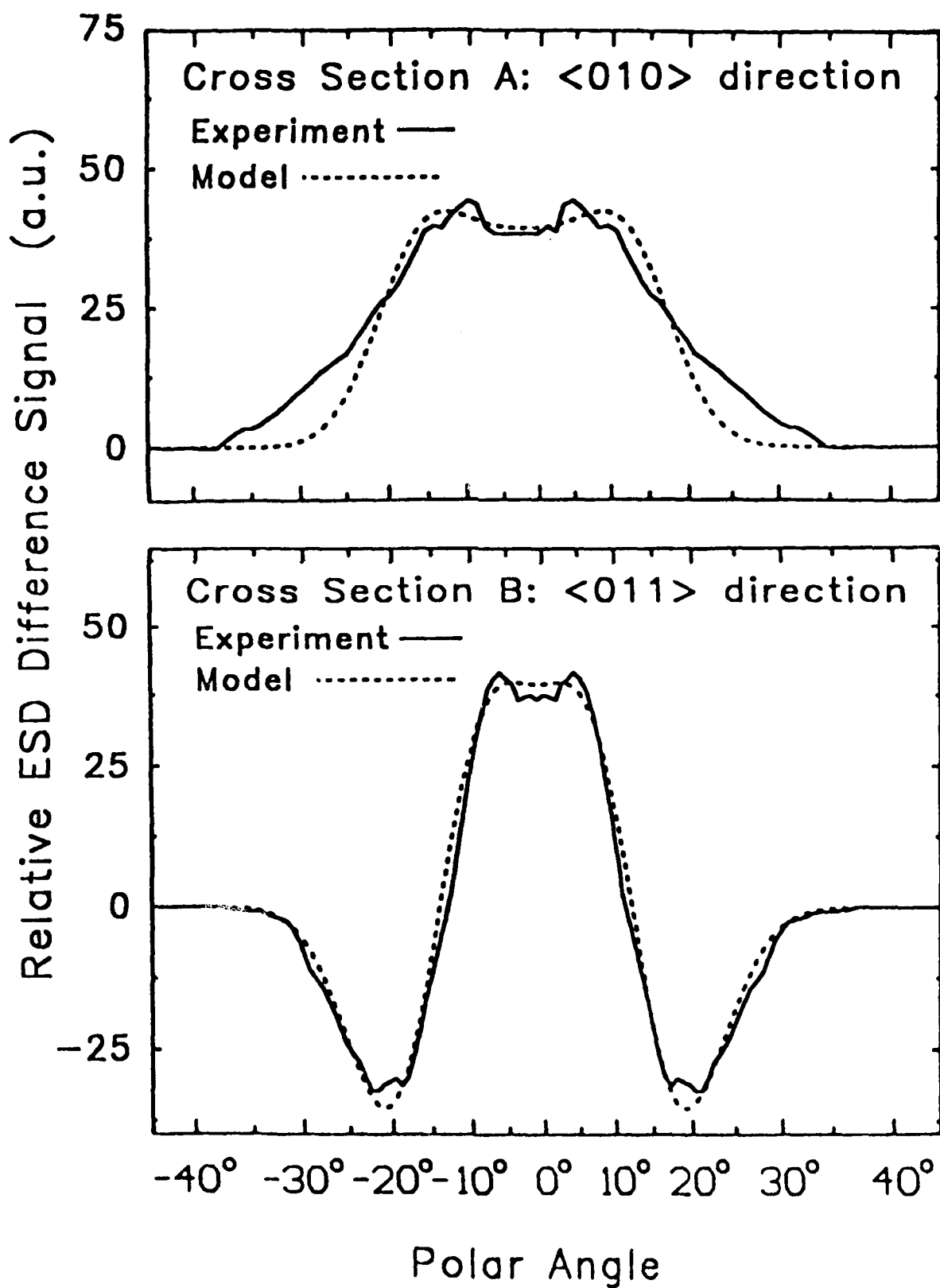
## (b) Model



# Cross Section Views of The Difference ESDIAD Patterns For Cl on Si(100)



# Cross Section Views of The Difference ESDIAD Patterns For OH on Si(100)



## ALF Contractor Distribution List

# Copies

D.T.I.C.

12

Bldg # 5, Cameron Station  
Alexandria, VA 22314

Dr. Andrew Freedman

1

Aerodyne Research, Inc.

45 Manning Road

Billerica, MA 01821

Tel: (508) 663-9500

FAX: (508) 663-4918

e-mail: aerodyn@mitvma.mit.edu

Dr. Asif Kahn

1

APA Optics

2950 NE 94th Lane

Blaine, MN 55434

Tel: (612) 784-4995

FAX: (612) 784-2038

e-mail: 70702.2032@compuserve.com

Dr. Duncan Brown

1

Advanced Technology Materials, Inc

7 Commerce Drive

Danbury, CT 06810

Tel: (203) 794-1100

FAX: (203) 792-8040

Dr. Peter Norris

1

EMCORE Corp.

35 Elizabeth Ave.

Somerset, NJ 08873

Tel: (201) 271-9090

Prof. Joe Greene

1

Dept. of Materials Science and Engineering

University of Illinois

1101 W. Springfield Ave.

Urbana, IL 61801

Tel: (217) 333-0747

Dr. T. P. Smith

1

IBM T.J. Watson Research Center

P. O. Box 218, Route 134

Yorktown Heights, NY 10598

e-mail: trey@ibm.com

Prof. Robert F. Davis

1

N.C.S.U. Box 7907

Raleigh, NC 27695-7907  
Tel: (919) 515-2377/3272  
FAX: (919) 515-3419  
e-mail: davis@mte.ncsu.edu

Prof. Salah Bedair 1  
Department of Electrical Engineering  
N.C.S.U.; Box  
Raleigh, NC 27695  
Tel: (919) 515-2336  
e-mail: jll@ecegrad.ncsu.edu

Max N. Yoder 1  
ONR Code 1114  
Arlington, VA 22217  
Tel: (703) 696-4218  
FAXes (703) 696-2611/3945/5383  
e-mail: yoder@charm.isi.edu

Dr. A. M. Goodman 1  
ONR, Code 1114  
Arlington, VA 22217  
Tel: (703) 696-4218  
FAXes (703) 696-2611/3945/5383  
e-mail: goodman@ocnr-hq.navy.mil

Dr. J. Pazik 1  
ONR Code 1113  
Arlington, VA 22217  
Tel: (703) 696-4410  
FAXes (703) 696-2611/3945/5383  
e-mail: pazik@ocnr-hq.navy.mil  
pazik@std.decnet@ccf.nrl.navy.mil

Prof. J. T. Yates, Jr. 1  
Dept. of Chemistry  
Surface Science Ctr.  
University of Pittsburgh  
Pittsburgh, PA 15260  
Tel: (412) 624-8320  
FAX: (412) 624-8552  
e-mail: yates@vms.cis.pitt.edu

Robert J. Markunas, R.A. Rudder 1  
Research Triangle Institute; Box 12194  
Research Triangle Park, NC 27709-2194  
Tel: (919) 541-6153  
FAX: (919) 541-6515  
e-mail: rjmk@rti.rti.org

Professor Mark P. D'Evelyn 1  
William Marsh Rice University  
Dept. of Chemistry  
P.O. Box 1892  
Houston, TX 77251  
Tel: (713) 527-8101, ext. 3468  
FAX: (713) 285-5155  
e-mail: mpdev@langmuir.rice.edu

Dr. Howard K. Schmidt 1  
Schmidt Instruments, Inc.  
2476 Bolsover, Suite 234  
Houston, TX 770054  
Tel: (713) 529-9040

FAX: (713) 529-1147  
e-mail: hksionwk@ricevml.rice.edu

Prof. A. F. Tasch 1  
Dept. of Electrical Engr. & Computer Science  
Engineering Science Bldg.  
University of Texas at Austin  
Austin, TX 78712  
Tel:  
FAX:  
e-mail: tasch@roz.ece.utexas.edu

Prof. Charles Tu 1  
Dept of Electrical & Computer Engr.  
UCSD  
LaJolla, CA  
Tel: (619) 534-4687  
FAX: (619) 534-2486  
e-mail: cwt@celece.ucsd.edu

Prof. John E. Crowell 1  
Department of Chemistry  
University of California at San Diego  
LaJolla, CA  
Tel: (619) 534-5441  
FAX: (619) 534-0058  
email: jcrowell@ucsd.edu

Prof. P. Daniel Dapkus 1  
University of Southern California  
University Park  
Los Angeles, CA 90089-1147  
e-mail: dapkus@mizar.usc.edu  
Tel: (213) 740-4414  
FAX: (213) 740-8684

Unless you are a small business invoking your 2 year proprietary rights clause, you MUST state on the front page of your report:  
Approved for Public Release; distribution unlimited.  
§

-----